

# *Ab initio* study of magnetic structure and chemical reactivity of $\text{Cr}_2\text{O}_3$ and its (0001) surface

Jason A. Cline<sup>†</sup>, Angeliki A. Rigos<sup>‡</sup>, Tomás A. Arias<sup>\*</sup>

<sup>†</sup>*Energy Laboratory and Department of Chemical Engineering,  
Massachusetts Institute of Technology, Cambridge, MA 02139.*

<sup>‡</sup>*Department of Chemistry,*

*Merrimack College, North Andover, MA 01845.*

<sup>\*</sup>*Laboratory for Atomic and Solid State Physics,  
Cornell University, Ithaca, NY 14853.*

(Submitted to the Journal of Physical Chemistry B on 6 December, 1999)

We present the first *ab initio* density functional theory study of the oxygen-terminated  $\text{Cr}_2\text{O}_3$  (0001) surface within the local spin-density approximation (LSDA). We find that spin plays a critical role for even the most basic properties of  $\text{Cr}_2\text{O}_3$  such as the structure and mechanical response of the bulk material. The surface exhibits strong relaxations and changes in electronic and magnetic structure with important implications for the chemical reactivity and unusual spin-dependent catalytic activity of the surface. Unlike the bulk, the outermost chromium bilayer is ferromagnetically ordered, and the surface oxygen layer exhibits appreciable net spin polarization in the opposite sense. Surprisingly, despite this ferrimagnetic order, the chemically important states near the Fermi level exhibit ferromagnetic order and thus favor electronic spin alignment of species interacting with the surface. Finally, we also find a high density of unoccupied electronic surface states available to participate in the chemical reactivity of the surface.

## I. INTRODUCTION

Chromium oxide is useful as a catalyst in many applications including internal combustion engine emission technology [1] and the dehydrogenation of alkanes [2,3]. It is also the primary constituent of passive films protecting stainless steels and other high performance industrial alloys [4-6]. Moreover, the surface is used in industry to catalyze the conversion of para- to ortho-hydrogen [7]. Intriguingly, this conversion has been observed to decrease by nearly an order of magnitude as the temperature increases through the Néel magnetic ordering temperature [8]. That this conversion is so efficient for a non-magnetic material such as  $\text{Cr}_2\text{O}_3$  has remained a subject of discussion for several decades [7]. Despite these intriguing and important phenomena, the surface electronic structure of  $\text{Cr}_2\text{O}_3$  is the least studied among the transition metal oxides [9].

Studies of corundum-structure metal oxides to date have neglected the electronic and magnetic structure of the surfaces of  $\text{Cr}_2\text{O}_3$ . Manassidis *et al.* [10] were one of the first to use *ab initio* density functional theory (DFT) within the local density approximation (LDA) to study the structure and energetics of basal plane surfaces of a corundum crystal ( $\text{Al}_2\text{O}_3$ ). They found very large surface relaxations which resulted in a reduction of the surface energy by a factor of two, but, as  $\text{Al}_2\text{O}_3$  is non-magnetic, whether transition metal systems exhibit this behavior remained unexplored. Veliah *et al.* [11] employed DFT with both the local spin-density approximation (LSDA) and non-local LSDA (NLSDA) to study  $\text{Cr}_m\text{O}_n$  clusters, but only up to  $m = 2, n = 3$ , too small to provide insight into the behavior of surfaces. Classical molecular dynamics calculations [12] as well as

*ab initio* periodic unrestricted Hartree-Fock (UHF) calculations of bulk  $\text{Cr}_2\text{O}_3$  [13] and its surface [14] have been carried out, but these studies have neglected the oxygen-terminated surface, which is important in oxygen-rich environments. Such surfaces have been studied, but in the related transition-metal material  $\alpha\text{-Fe}_2\text{O}_3$ . Using spin-DFT within the generalized gradient approximation and a full potential linearized augmented plane wave (FP-LAPW) basis set, Wang *et al.* [15] studied the  $\alpha\text{-Fe}_2\text{O}_3$  (0001) surface as a function of increasing oxygen pressure and demonstrated that, indeed, the oxygen-terminated surface eventually becomes the most stable.

To better understand the unique properties of  $\text{Cr}_2\text{O}_3$ , we explore the oxygen-terminated (0001) surface of  $\text{Cr}_2\text{O}_3$  using the *ab initio* plane-wave pseudopotential approach within LSDA. Section II briefly reviews our methodology, and Section III A gauges the reliability of this approach through detailed comparisons with experimental information on the lattice constant, bulk modulus, and atomic arrangement and magnetic structure of the bulk material. Finally, in Section III B, we contrast the atomic, electronic, and magnetic structures of the surface with those of the bulk.

## II. METHODOLOGY

Our calculations are carried out within the *ab initio* pseudopotential density-functional formalism which has been applied successfully in the past to a wide variety of solid state and surface systems. (See [16] for a review.) The present calculations involve three primary approximations: the local density approximation to density functional theory, the pseudopotential (“frozen-

core”) approximation and the supercell approximation.

To evaluate the efficacy of local density functionals in treating the present material, we have calculated the properties of bulk  $\text{Cr}_2\text{O}_3$  within both LDA and LSDA as parameterized in [17] and [18], respectively. These results (Section III A) show that LSDA gives a description far superior to the LDA and also gives results better than those reported in the literature for unrestricted Hartree-Fock (UHF) calculations [13]. Accordingly, we employ LSDA exclusively for the surface calculations below.

To represent the chromium and oxygen ionic cores in this study, we employ pseudopotentials of the non-local Kleinmann-Bylander separable form [19] as generated using the optimized pseudopotential procedure of Rappe et al. [20]. Preliminary calculations carried out on small atomic clusters indicate that the states of the argon shell are relatively close in energy to the  $2s$  states of oxygen. Out of concern for the possible mixing of the argon-shell electrons of chromium with the oxygen valence shell, we include the argon-shell electrons explicitly in our calculation as valence electrons and pseudize only the neon core of chromium in our pseudopotential. Convergence tests show that both this pseudopotential and that for oxygen are well-converged at a plane wave cutoff of 80 Rydbergs, which we use for all results reported below. We find that, relative to the argon-core pseudopotential, the neon-core potential reduces errors in the band structure relative to the results of LAPW calculations [21] by a factor of two.

For the bulk calculations described below, we employ the ten-atom corundum primitive cell of  $\text{Cr}_2\text{O}_3$ . For this cell, we sample the Brillouin zone with an eight k-point Monkhorst-Pack [22] mesh, which folds to four points under time-reversal symmetry. This corresponds to a reciprocal-space sampling density of  $0.37 \text{ bohr}^{-1}$ , which is commonly used to treat silicon and which we expect to be more than sufficient for this even more ionically bonded system.

For the surface calculations, we employ the supercell approach with periodic boundary conditions in all three dimensions, thereby allowing us to study isolated slabs of  $\text{Cr}_2\text{O}_3$  material with two (0001) surfaces separated by  $7 \text{ \AA}$  of vacuum. This supercell contains five bilayers of chromium and six layers of oxygen. We arrange these to form a slab with two identical oxygen-terminated surfaces in a unit cell with the in-plane lattice constant held at the *ab initio* value. Such slabs were found sufficient for studies of the corresponding surface of  $\text{Fe}_2\text{O}_3$  [15] and avoid the formation of a net electric dipole in the supercell. For the surface cells, we use four k-points (which fold to two) in the plane perpendicular to the  $c$ -axis of the cell. This yields a reciprocal space sampling comparable to that of our bulk calculations.

Within the above approximations, we determine the quantum state of the system by minimizing the total energy over all possible sets of orthonormal electronic wavefunctions using the analytically-continued functional approach [16,23], which has been recently shown to be nearly optimal in a rigorous mathematical sense [24]. The

calculations are performed within the DFT++ formalism [25,26] which makes different physical descriptions (LDA, LSDA, SIC, Hartree-Fock, etc.) relatively simple to explore and provides both high portability and good computational performance. Finally, when determining structures, we relax the atomic coordinates until the Hellmann-Feynman forces on the atomic cores are less than  $0.03 \text{ eV/\AA}$  in each coordinate direction.

### III. RESULTS AND DISCUSSION

#### A. Bulk $\text{Cr}_2\text{O}_3$

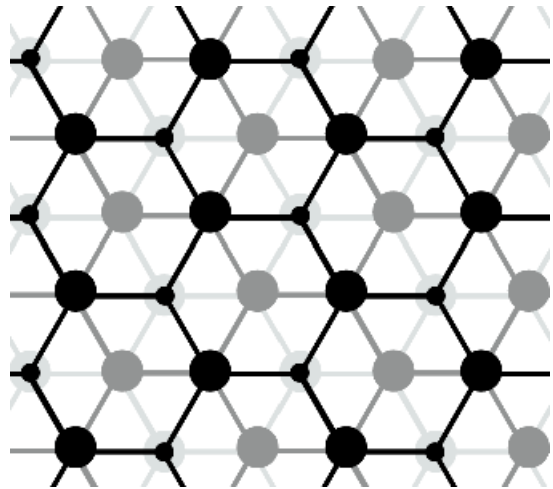


FIG. 1. Schematic projection of the metallic atoms in the corundum structure, viewed atop the (0001) surface, showing chromium atoms only. The chromium atoms in the structure are colored according depth and are arranged in a sequence of bilayers with honeycomb structure (three are shown). The upper and lower chromium atoms of each bilayer appear as large and small circles, respectively.

The crystal structure of  $\text{Cr}_2\text{O}_3$  is important for understanding the relaxation of the internal coordinates of the unit cell, the magnetic order of the bulk, and the structure of the surface.  $\text{Cr}_2\text{O}_3$  assumes a corundum-type structure (space group  $R\bar{3}c$ ), which has a ten-atom primitive cell that is equivalent to a thirty-atom cell on a hexagonal lattice. The structure consists of alternating oxygen layers and chromium bilayers stacked along the  $c$ -axis of the hexagonal lattice. Figure 1 shows the arrangement of the chromium bilayers. Each bilayer consists of two perfectly planar triangular lattices arranged so that their combined projection forms an ideal honeycomb structure whose two-element basis consists of one atom from each sublattice. The difference between the crystallographic parameter “ $z(\text{Cr})$ ” [27] and one-third measures the separation of the planes which make up the bilayer. In the structure, the chromium bilayers align in an ABC stacking sequence along the  $c$ -axis such that atoms from

the furthest sublayers of each bilayer pair align directly along the  $c$ -axis. All oxygen atoms in a layer lie in exactly the same plane and form an approximate triangular lattice. The difference between the crystallographic parameter “ $x(\text{O})$ ” [27] and one-third measures a slight contraction of those triangles in this lattice which are centered on  $c$ -axis aligned pairs of chromium atoms.

It is known experimentally that, unlike  $\text{Fe}_2\text{O}_3$  and  $\text{V}_2\text{O}_3$ , both  $\text{Al}_2\text{O}_3$  and  $\text{Cr}_2\text{O}_3$  contract nearly isotropically (within tenths of a percent) under hydrostatic pressure [28]. Accordingly, for our LDA and LSDA calculations, we determined bulk moduli and unit cell volume by holding the ratio  $c/a$  between the hexagonal crystal axes constrained to the experimental value of 2.7407 [29, p. 469]. At each volume, we optimized the internal coordinates of the unit cell, and applied a standard Pulay stress correction [30,31] for changes in finite-basis size to the resulting total energy. The minimum energy, location of the minimum and the second derivative of the energy as a function of lattice constant give the cohesive energy, unit-cell volume and bulk modulus, respectively.

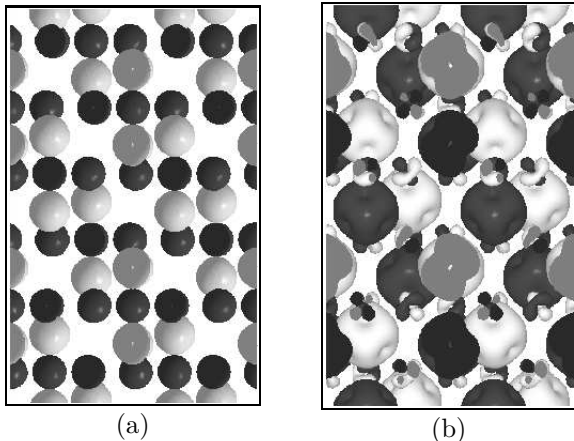


FIG. 2. LSDA predictions for a thirty atom cell of bulk  $\text{Cr}_2\text{O}_3$ . Left panel (a) shows a single isosurface of the predicted total electron density ( $n_\uparrow + n_\downarrow$ ), with the surface colored according to proximity to chromium atoms (white) and oxygen atoms (charcoal). Right panel (b) shows the spin polarization,  $n_\uparrow - n_\downarrow$ , for bulk  $\text{Cr}_2\text{O}_3$  within LSDA (thirty atom calculation): contour of net up-spin (white), contour of net down-spin (charcoal). For both panels some atoms are cut-off at the cell boundary, revealing darker shaded interiors.

Table I compares our results for bulk modulus, unit cell volume, cohesive energy (atomization energy to neutral atoms), and internal cell coordinates with experiment and unrestricted Hartree-Fock results [13]. Whereas the LDA calculations are in error by about -10% and 44% for unit cell volume and bulk modulus, respectively, the corresponding errors for UHF are +5% and +13% and for LSDA are -1.7% and within experimental error (5%), respectively. Moreover, in going from LDA to LSDA, the error of the cohesive energy, determined from Born-Haber cycle data for  $\text{Cr}_2\text{O}_3$  [32] and the bond strength of molec-

ular oxygen [33], reduces from -12% to -6%. (Ref. [13] does not provide a value of the cohesive energy.)

We find that the LDA prediction of the internal coordinates of the unit cell is in significant error. We note that  $x(\text{O})$  for the LDA structure is nearly one-third, indicating a tendency toward a perfect triangular lattice in each O layer. Our LSDA results, on the other hand, are in much better accord with experiment, showing even somewhat better agreement than reported for UHF [13]. The uncertainties quoted for  $x(\text{O})$  and  $z(\text{Cr})$  in the table represent small differences in position of equivalent atoms due to numerically imperfect relaxation.

Given the success of the LSDA description and its clear superiority over the LDA (and UHF), all results reported below are computed within LSDA.

Next, we turn our attention to the magnetic structure of bulk  $\text{Cr}_2\text{O}_3$ . Figure 2b presents our prediction for the ground-state spin density. Consistent with expectations, we find that the spin polarization in the bulk material concentrates almost entirely on the chromium atoms (large dimpled contours in the figure). The spin order is antiferromagnetic among nearest neighbors in each chromium bilayer, leading to an intra-layer order in which the spin direction is constant in each sublayer. Moreover, we find an inter-layer order such that the spin-up/spin-down sequence along the  $c$ -axis is identical for each bilayer. These results are in complete accord with the magnetic order inferred from neutron diffraction experiments [34]. Finally, we find that the oxygen atoms have lobes of opposite spin-polarization with negligible net spin.

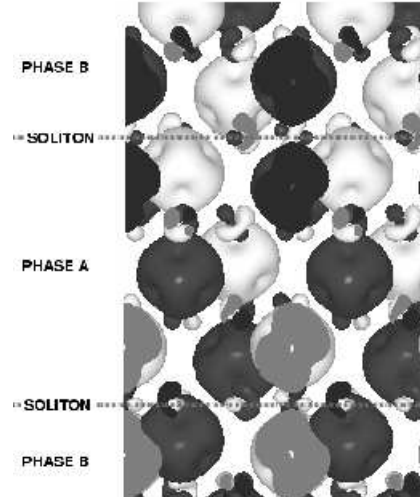


FIG. 3. Antiferromagnetic soliton in  $\text{Cr}_2\text{O}_3$  within LSDA (same conventions as in Figure 2b).

To confirm that the state shown in Figure 2b as the ground state within LSDA, we relaxed our initial electronic state from completely random wavefunctions. This resulted in a spin state in which the magnetic order

within each bilayer was the same as described above, suggesting that the antiferromagnetic intra-layer order is quite stable. However, in this calculation, the spin-up/spin-down sequence of the bilayers reversed from one ground state to the spin-flip related phase. (See Figure 3.) This corresponds to the presence of two antiferromagnetic solitons in the supercell. LSDA ascribes a positive energy to this excitation, indicating that the spin ordering shown in Figure 2b represents the ground state. From our results, we extract the first *ab initio* estimate for the (0001) *c*-axis antiferromagnetic coupling constant,  $J_{AB} \approx 150 \text{ cm}^{-1}$ . Experiments provide highly variable estimates for this coupling constant from about  $J_{AB} \approx 250 \text{ cm}^{-1}$  to  $\approx 350 \text{ cm}^{-1}$  [35].

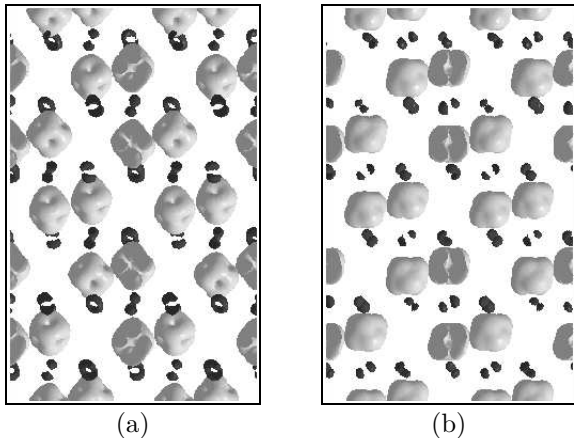


FIG. 4. Local chemical softness map of bulk  $\text{Cr}_2\text{O}_3$ . Portrayed are the HOMOs (a) and LUMOs (b) as calculated within LSDA. The figure shows a single isosurface of local softness, which is colored according to proximity to either chromium (white) or oxygen (charcoal) atoms.

Finally, Figure 4 shows contour surfaces of the electron density of the highest occupied molecular orbitals (HOMOs) and the lowest unoccupied molecular orbitals (LUMOs), representing the local chemical softness [36]. Species which tend to accept or donate electrons tend toward regions with strong HOMO or LUMO concentration, respectively. The figure shows that, in bulk, the chromium atoms interact with either type of species, whereas the oxygen atoms are relatively inert.

### B. Oxygen-terminated (0001) surface

Comparing the relaxed surface slab to the bulk, we find that the primary structural change is a significant motion of surface oxygen atoms (layer O[1] in Figure 5a) toward the outermost sublayer of chromium atoms (layer Cr[2a]). This motion involves both a vertical component perpendicular to the surface and a lateral component in the surface plane. The vertical component reduces the interplanar spacing of layers O[1] and Cr[2a] by 33%. The

lateral component rotates triangles of oxygen atoms centered above the chromium atoms of layer Cr[2b] by  $6.5^\circ$ , similar to the rotation of  $10^\circ$  reported for  $\text{Fe}_2\text{O}_3$  [15]. The second most significant change is an increase of 9%, or  $0.12 \text{ \AA}$ , in the distance between the chromium layer Cr[2b] and the next deeper oxygen layer O[3]. All shifts deeper within the structure are less than  $0.06 \text{ \AA}$ . Table II summarizes our results.

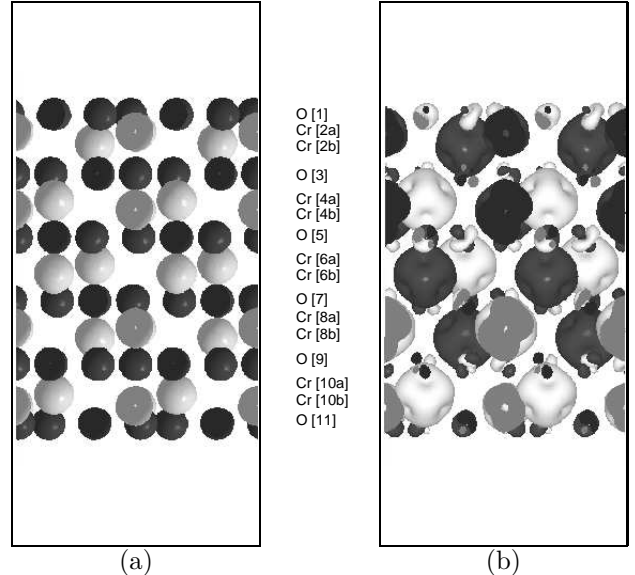


FIG. 5. LSDA predictions for a twenty-eight atom surface slab of  $\text{Cr}_2\text{O}_3$ : electron density (a) and spin polarization (b) (same conventions as Figure 2.)

The magnetic structure of the surface is significantly different from that of the bulk (Figure 5b). The most striking feature is that the outermost chromium bilayer is now ferromagnetically ordered. In addition, we find a noticeable spin moment on the outermost *oxygen* layer in the opposite spin orientation, similar to what has been found in  $\text{Fe}_2\text{O}_3$  [15]. From the figure, it is clear that the origin of the net spin of the outer oxygen atoms is the de-population of the lobes of opposing spin, which are normally filled in the bulk.

In order to understand the chemical reactivity of the  $\text{Cr}_2\text{O}_3$  surface, we compare the HOMO and LUMO states of the surface slab in Figure 6a and 6b. These figures show a remarkable spatial separation between the HOMOs and LUMOs. The HOMO states, which would interact most strongly with electron-accepting species such as protons, contract into the bulk and leave almost no concentration on the outer oxygen atoms. On the other hand, the LUMO states, which interact with electron-donating species such as chloride or sulfide ions, concentrate strongly on the surface. This suggests that such electron-donating species would be more disruptive to the surface than would be their electron-accepting counterparts.

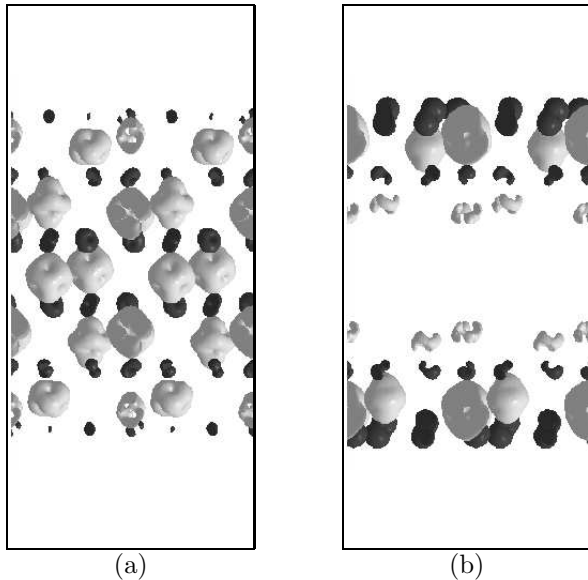


FIG. 6. Local chemical softness map for the surface slab of  $\text{Cr}_2\text{O}_3$ : HOMOs (a), LUMOs (b). Colors indicate proximity to chromium (white) and oxygen (charcoal).

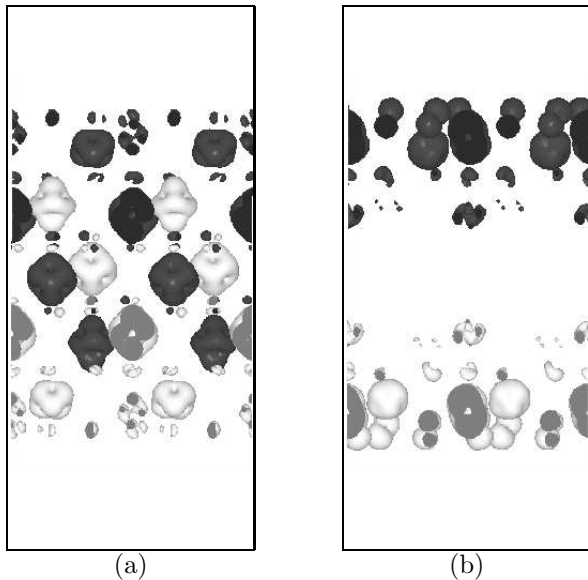


FIG. 7. Spin-dependence of the local chemical softness map for the surface slab of  $\text{Cr}_2\text{O}_3$ : HOMOs (a), LUMOs (b). Colors indicate spin direction.

The spin polarization of the HOMOs and LUMOs on the chromium atoms mimics the ferromagnetic behavior of the total spin density, as one would expect from Hund's rule. (See Figure 7.) However, the HOMO and LUMO states of the oxygen atoms spin polarize oppositely to the total spin density. The reactive states of the surface are thus uniformly spin polarized and provide an environment which encourages alignment of the electronic spins of adsorbed species. This provides an intriguing starting point for understanding the conversion of para- to ortho-

hydrogen which has been observed to occur more readily in the presence of magnetically ordered surfaces of  $\text{Cr}_2\text{O}_3$  [8].

#### IV. CONCLUSIONS

The preceding results for the bulk crystal establish the critical role of spin in the physics and chemistry of  $\text{Cr}_2\text{O}_3$ . We show that the plane-wave pseudopotential LSDA approach gives a good description of the structure, mechanical response and magnetic order of the bulk. Through this approach, we provide the first *ab initio* estimate of the antiferromagnetic coupling constant.

The oxygen-terminated (0001) surface of  $\text{Cr}_2\text{O}_3$  exhibits strong inward relaxation of the outermost oxygen layer with an associated rotational reconstruction, as has been found in previous theoretical studies of similar materials. Understanding surface processes such as catalysis and corrosion initiation, however, requires fundamental knowledge of the electronic structure and cannot be inferred from the surface relaxation alone.

We find that the electronic structure of the surface differs radically from that of the bulk. In particular, the outermost chromium bilayer does not exhibit the antiferromagnetic order of the bulk but is ordered ferromagnetically. Moreover, the outer oxygen layer, rather than exhibiting zero net spin polarization, develops an appreciable net spin, but in the sense opposite to that of the underlying ferromagnetic chromium bilayer. Additionally, the surface manifests a high density of low-energy unoccupied electronic states available to influence chemical reactions at both oxygen and chromium surface sites, but with negligible penetration into the bulk. There is also some density of high-energy occupied states reaching outward from the bulk into the outermost chromium bilayer. Remarkably, although the spins of the outermost oxygen and chromium atoms orient in opposite directions, the chemically relevant electronic states create a blanketing environment of uniform spin which is available to encourage spin alignment of adsorbed species. This new understanding provides a path for insight into novel magneto-chemical effects and their implications for catalysis.

#### ACKNOWLEDGMENTS

This work is partially supported by the National Computational Science Alliance under Proposal #DMR980011N and utilizes the Boston University SGI/CRAY Origin2000. J.A.C. gratefully acknowledges funding provided by the Army Research Office under the University Research Initiative (Projects 30345-CH-URI and 34173-CH-AAS, grant numbers DAAL03-92-G-0177 and DAAH04-95-1-0302). A.A.R. was partially funded by a Merrimack College Faculty Development Grant.

Thanks also to J. W. Tester, R. M. Latanision, D. B. Mitton, M. T. Reagan, P. A. Marrone, S. Ismail-Beigi, D. Yesiltepe for their help in a wide variety of capacities, and to C. N. Hill and the MIT Lab for Computer Science for use of the Pleiades Alpha-cluster.

- 
- [1] P. G. Harrison, N. C. Lloyd, and W. Daniell. *J. Phys. Chem.*, 102:10672, 1998.
- [2] G. C. Bond. *Heterogeneous Catalysis: Principles and Applications*. Oxford Chemistry Series. Clarendon Press, Oxford, 1974.
- [3] L. R. Mentastay, O. F. Gorrioz, and L. E. Cadus. *Ind. Eng. Chem. Res.*, 38:396, 1999.
- [4] N. C. Alstrup, N. Langrad, and I. Chorkendorff. *Surface and Interface Analysis*, 22(1):441–4, July 1994.
- [5] M. O. Figueiredo, A. Correia dos Santos, H. Carmezim, M. Abbate, F. M. F. deGroot, H. Petersen, and W. Braun. *Analyst*, 119:609, 1994.
- [6] M. P. Ryan, R. C. Newman, and G. E. Thompson. *Philosophical Mag. B*, 70(2):241–51, August 1994.
- [7] Ernest Ilisca. *Prog. in Surf. Sci.*, 41:217–335, 1992.
- [8] J. A. Arias and P. W. Selwood. *J. Catal.*, 30:255–9, 1973.
- [9] V. E. Henrich and P. A. Cox. *The Surface Science of Metal Oxides*. Cambridge University Press, Cambridge, 1994.
- [10] I. Manassidis, A. De Vita, and M. J. Gillan. *Surf. Sci. Lett.*, 285:L517, 1993.
- [11] S. Veliah, K-H Xiang, R. Pandey, J. M. Recio, and J. M. Newsam. *J. Phys. Chem. B*, 102:1126, 1998.
- [12] F. Rohr, M. Bäumer, H.-J. Freund, J. A. Meijas, V. Staemmler, S. Müller, L. Hammer, and K. Heinz. *Surface Science*, 372:L291–L297, 1997.
- [13] M. Catti, G. Sandrone, G. Valerio, and R. Dovesi. *J. Phys. Chem. Solids*, 57:1735, 1996.
- [14] C. Rehbein, F. Michel, N. M. Harrison, and A. Wander. *Surface Review and Letters*, 5(1):337–40, 1998.
- [15] X.-G. Wang, W. Weiss, Sh. K. Shaikhutdinov, M. Ritter, M. Petersen, F. Wagner, R. Schlögl, and M. Scheffler. *Phys. Rev. Lett.*, 81(5):1038–1041, August 1998.
- [16] M. C. Payne, M. P. Teter, D. C. Allan, T. A. Arias, and J. D. Joannopoulos. *Reviews of Modern Physics*, 64(4):1045–97, 1992.
- [17] Z. Szotek, W. M. Temmerman, and H. Winter. *Phys. Rev. B*, 47:4029, 1993.
- [18] J. P. Perdew and Yue Wang. *Phys. Rev. B*, 45:13244, 1992.
- [19] L. Kleinman and D. M. Bylander. *Phys. Rev. Lett.*, 4:1425, 1982.
- [20] A. M. Rappe, K. M. Rabe, E. Kaxiras, and J. D. Joannopoulos. *Phys. Rev. B*, 41:1227, 1990.
- [21] D. A. Papaconstantopoulos. *Handbook of the Band Structure of Elemental Solids*. Plenum Press, New York, 1986.
- [22] H. J. Monkhorst and J. D. Pack. *Phys. Rev. B*, 13:5188, 1976.
- [23] T. A. Arias, M. C. Payne, and J. D. Joannopoulos. *Phys. Rev. Lett.*, 69(7):1077–80, August 1992.
- [24] Alan S. Edelman, Tomás A. Arias, and Steven T. Smith. *Society for Industrial and Applied Mathematics Journal on Matrix Analysis and Applications*, 20:303, 1998.
- [25] Sohrab Ismail-Beigi and T. A. Arias. In Charles E. Leiserson, editor, *Proceedings of the 1998 MIT Student Workshop on High-Performance Computing in Science and Engineering*, number 737. MIT Laboratory for Computer Science, 1998.
- [26] T. A. Arias. *Reviews of Modern Physics*, 71(1):267–311, January 1999.
- [27] Theo Hahn, editor. *International Tables for Crystallography*, volume A. Kluwer Academic Publishers, Boston, 1995.
- [28] Y. Sato and S. Akimoto. *J. Appl. Phys.*, 50:5285, 1979.
- [29] K.-H. Hellwege, editor. *Crystal Structure Data of Inorganic Compounds*, volume 7 of *Landolt-Börnstein*. Springer-Verlag, Berlin, 1975.
- [30] S. Froyen and M. L. Cohen. *J. Phys. C*, 19:2623, 1985.
- [31] P. Gomez Dacosta, O. H. Nelson, and K. Kunc. *J. Phys. C*, 19:3163, 1986.
- [32] Jack Sherman. *Chemical Reviews*, 11(1):93–170, 1932.
- [33] David R. Lide, editor. *CRC Handbook of Chemistry and Physics*. CRC Press, New York, 79th edition, 1999.
- [34] B. N. Brockhouse. *J. Chem. Phys.*, 21:961–2, 1953.
- [35] C. P. Poole and J. F. Itzel. *J. Chem. Phys.*, 41(2):287–95, July 1964.
- [36] W. Yang and R. G. Parr. *Proc. Natl. Acad. Sci. USA*, 82:6723, 1985.
- [37] L. W. Finger and R. M. Hazen. *J. Appl. Phys.*, 51:5362, 1980.
- [38] H. Sawada. *Materials Research Bulletin*, 29(3):239–45, 1994.

| Model                         | $B$ (Mbar) | $V$ ( $\text{\AA}^3$ ) | $E$ (eV)           | $1/3 - x(\text{O})$ | $z(\text{Cr}) - 1/3$ |
|-------------------------------|------------|------------------------|--------------------|---------------------|----------------------|
| LDA                           | 3.39(10)   | 43.34(04)              | 23.63              | -0.004(2)           | 0.00626(1)           |
| LSDA                          | 2.35(12)   | 47.19(14)              | 25.24              | 0.03133(8)          | 0.01647(1)           |
| UHF                           | 2.66(10)   | 50.5                   | —                  | 0.03273             | 0.01722              |
| Published Experimental Values |            |                        |                    |                     |                      |
| Ref. [37]                     | 2.38(12)   | 47.997(5)              | —                  | —                   | —                    |
| Ref. [28]                     | 2.31(30)   | 48.0                   | —                  | 0.0282              | 0.01437              |
| Ref. [32]                     | —          | —                      | 26.87 <sup>†</sup> | —                   | —                    |
| Ref. [38]                     | —          | —                      | —                  | 0.02763             | 0.01417              |

<sup>†</sup> Computed with Born-Haber cycle. (See Text.)

TABLE I. Comparison of computed bulk moduli  $B$ , volume per formula unit  $V$ , cohesive energy  $E$ , and internal cell coordinates  $x$  and  $z$  in ten-atom cell of  $\text{Cr}_2\text{O}_3$  with experimental values. Volume and cohesive energies (relative to isolated atoms) are per  $\text{Cr}_2\text{O}_3$  formula unit.

| Layer pair    | Bulk spacing [ $\text{\AA}$ ] | Surface spacing [ $\text{\AA}$ ] |
|---------------|-------------------------------|----------------------------------|
| O[1]–Cr[2a]   | 0.94                          | 0.63                             |
| Cr[2a]–Cr[2b] | 0.39                          | 0.40                             |
| Cr[2b]–O[3]   | 0.94                          | 1.05                             |
| O[3]–Cr[2b]   | 0.94                          | 0.92                             |

TABLE II. *Ab initio* prediction of changes in interlayer spacing at the (0001)  $\alpha$ - $\text{Cr}_2\text{O}_3$  surface.